Cross-validation of microfabricated atomic magnetometers with superconducting quantum interference devices for biomagnetic applications

Svenja Knappe,[1,a)] Tilmann H. Sander,[2] Olaf Kosch,[2] Frank Wiekhorst,[2] John Kitching,[1] and Lutz Trahms[2]
[1]*NIST, Time and Frequency Division, 325 Broadway, Boulder, Colorado 80305, USA*
[2]*Physikalisch-Technische Bundesanstalt, Abbestr. 2-12, 10587 Berlin, Germany*

(Received 8 June 2010; accepted 27 August 2010; published online 28 September 2010)

We compare the performance of a chip-scale atomic magnetometer (CSAM) with that of a superconducting quantum interference device (SQUID) sensor in two biomedical applications. Magnetocardiograms (MCGs) of healthy human subjects were measured simultaneously by a CSAM and a multichannel SQUID sensor in a magnetically shielded room. The typical features of MCGs are resolved by the CSAM, matching the SQUID results. Magnetorelaxometry (MRX) signals of iron nanoparticles were also obtained with the CSAM and compared to similar measurements with a SQUID. © *2010 American Institute of Physics*. [doi:10.1063/1.3491548]

The field of biomagnetic measurements is largely dominated by magnetic sensors based on superconducting quantum interference devices (SQUIDs). The high sensitivity of these devices in the frequency band from 1 Hz to 1 kHz enables measurements of many biologically relevant magnetic sources inside the human body,[1] as well as low field magnetic resonance imaging.[2] In addition, SQUIDs are used in magnetorelaxometry (MRX),[3] which provides a quantitative and spatially resolved imaging through the detection of magnetic nanoparticles.

Because SQUIDs require cryogenic cooling, which implies significant cost and operational complexity, it is desirable to investigate the use of alternative sensors for some of these measurements. Recently, magnetometers based on the precession of atomic spins have demonstrated sensitivities (noise equivalent magnetic field) of 0.2 $\mathrm{fT}/\mathrm{Hz}^{1/2}$ in laboratory settings over a limited frequency range.[4] With these atomic or optical magnetometers, measurements of the magnetic fields produced by the human brain[5] and heart[6] have been carried out. These instruments are based on glass-blown vapor cells with volumes of several thousand cubic millimeters; a complete measurement apparatus typically occupies several tens of liters.

Chip-scale atomic magnetometers (CSAMs) (Ref. 7) are based on microfabricated, millimeter-scale alkali vapor cells integrated with small optical components such as diode lasers and fiber optics. These devices have reached sensitivities below 5 $\mathrm{fT}/\mathrm{Hz}^{1/2}$ at 100 Hz in tabletop setups[8] and the fundamental sensitivity limits are better than this by more than an order of magnitude.[9] Advantages of these sensors over larger conventional optical magnetometers include lower-power operation, the possibility of low-cost manufacturing of large arrays, the arrangement in flexible or conformal geometries around the magnetic field source to be measured, a higher intrinsic bandwidth and enhanced proximity to sources.

In this paper we investigate the use of an optical fiber-coupled CSAM in two typical biomagnetic measurements, magnetocardiogram (MCG) and MRX. Simultaneous measurements of biomagnetic signals from humans with the CSAM and a SQUID allow a clear comparison of these two sensors in a typical biomagnetic measurement setting. The continuous raw signals obtained by the CSAM show many features present in the SQUID measurements and confirm that CSAMs are a promising technology for biomagnetic applications.

The CSAM consisted of a microfabricated silicon/glass sensor head of volume 0.75 cm^3, coupled to a portable control box by optical fibers of length 5 m. At the heart of the sensor head was cell of volume 8 mm^3 containing $^{87}\mathrm{Rb}$ atoms along with roughly 1 amagat of nitrogen. The distance between the center of the vapor cell and the outside of the sensor head housing was 2.5 mm, defining the minimum distance of the sensitive volume from a magnetic source. Thermal isolation enabled the outside surface of the sensor to remain at room temperature, while the cell was heated to 150 °C. Details of the fabrication and design of the sensor can be found elsewhere.[10]

The laser light transmitted through the fibers optically pumped the atoms into an oriented state and simultaneously probed the effects of the magnetic field.[9] The CSAM achieved sensitivities of several hundred $\mathrm{fT}/\sqrt{\mathrm{Hz}}$ at frequencies between 10 and 100 Hz when operated at low magnetic fields and high alkali densities, where spin-exchange collisions between the Rb atoms can be suppressed.[11]

In order to reduce 1/f noise in the optical sensor, an alternating transverse magnetic field at 2.2 kHz was applied to the sensor head by use of a pair of small coils outside of the sensor.[10] A dispersive resonance signal was detected with phase-sensitive detection at 2.2 kHz. A bias field cancelled any residual static background field and tuned the magnetometer to the zero crossing of this resonance. The lock-in output was then proportional, over a range of roughly 100 nT, to the time-varying component of the local magnetic field that was parallel to the modulation field.

Biomagnetic fields were measured with the CSAM and simultaneously with a multichannel low-temperature SQUID magnetometer system.[12] The experiment was performed inside the magnetically shielded room BMSR-2.[13] For the

[a)]Also with University of Colorado, Boulder 80309, USA.

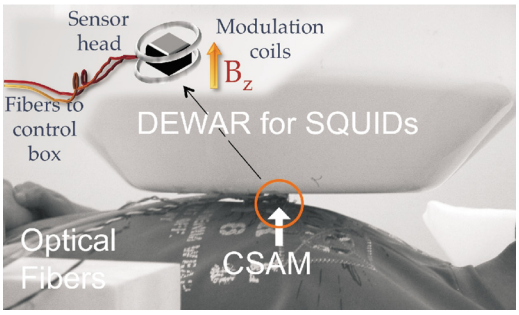

FIG. 1. (Color online) Photograph of the measurement setup from the side. The CSAM is attached to the bottom of the Dewar containing the SQUID sensors. The optical fibers are fed to a control unit outside the shielded room. The Dewar can be positioned freely above the chest of the subject. (Top left inset) Schematic of the CSAM arrangement. Modulation coils around the sensor head allow the measurement of the z-component of the magnetic field.

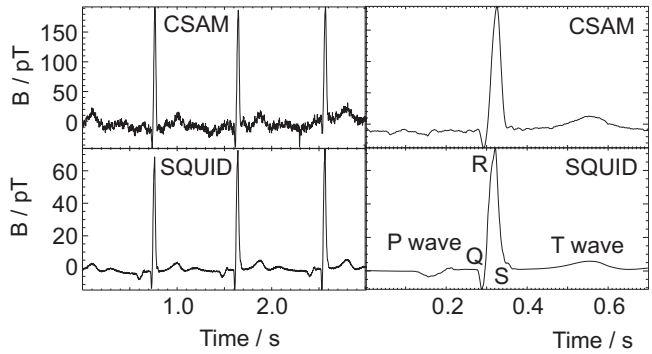

FIG. 2. Raw MCG signal of a subject detected simultaneously with (a) the CSAM and (b) a SQUID. Averaged MCG signal (200 beats) of the same person measured simultaneously with (c) the CSAM and (d) a SQUID.

MCG measurements the CSAM sensor head was mounted directly underneath the center of the SQUID array in which 57 SQUIDs were arranged in a plane at the Dewar bottom. These SQUIDs measured the (vertical) z-component of the cardiomagnetic field. The modulation field of the CSAM distorted the signal of the central sensors in the bottom plane of the SQUID array but the 45 sensors located several centimeters from the CSAM operated normally.

The CSAM was positioned directly above the left chest of a recumbent male human subject and the z-component of the magnetic field, perpendicular to the subject's torso, was measured. The intrinsic bandwidth of the CSAM was roughly 1 kHz, limited by the width of the resonance line, and the lock-in integration time constant was set to 1 ms. The CSAM control box was placed outside the shielded room, yet within the rf shield, and the optical fibers connecting the control box to the sensor head were routed through small holes to the interior (Fig. 1).

The CSAM output signal was calibrated independently with two coils in the vicinity of the sensor. The output of the CSAM and 45 SQUID magnetometers oriented in the z direction were simultaneously recorded at 1000 samples/s, and an antialiasing filter was set below 500 Hz. A digital phase-adapted sine-wave filter was used to suppress power line interference at 50 and 100 Hz in the CSAM signal. This interference was most likely caused by the heater power supply. Several runs were performed on two subjects at different positions over the chest, each recording lasting for 5 min.

Continuous raw data are shown in Figs. 2(a) and 2(b) for one of the off-center SQUIDs and the CSAM. The QRS-complex is clearly visible in both data sets, as well as the T-wave. It can be seen that the optical sensor exhibits more noise than the SQUID sensor. The higher noise is partly offset by larger signal amplitudes due to the proximity of the optical sensor to the chest of the subject, with a distance of only 5 mm between sensor and skin. The CSAM R-peak is roughly three times stronger than the corresponding SQUID signal. This is in agreement with an inverse cubic field attenuation with distance and estimated distances between CSAM and heart of 5.0 cm and SQUID and heart of 7.5 cm. In order to average the data, a threshold was placed on the value of the R-peak in the signal of one of the SQUID sensors. The time that the signal crossed this threshold was used as a trigger to synchronize the signals for averaging. An average over 200 beats is shown in Figs. 2(c) and 2(d). Now detailed features of the QRS-complex and the T-wave are clearly visible. The P-wave exhibits a morphology clearly different from the SQUID-MCG, probably due to the difference in location between SQUID and CSAM. Besides the SQUID-MCG shown here 45 other channels were measured encircling the CSAM, which was placed centrally below the SQUID array. The P-wave shows a gradual change across the SQUID array signals and the morphology of the CSAM P-wave is consistent with this. These measurements demonstrate the similar capabilities of the two types of sensors and validate the signal recorded with the CSAM.

MRX refers to measurements of the magnetization decay of magnetic nanoparticles after removal of a magnetizing field that initially aligns their magnetic moments.[3] The relaxation signals are specific to the magnetic nanoparticles without any interference from surrounding tissue backgrounds and their amplitudes are proportional to the iron content in the nanoparticle sample. Two different thermally induced relaxation processes can be distinguished: The Brownian relaxation process in which rotation of the nanoparticles results in a decay of the magnetization of the sample with a relaxation time τ_B that is proportional to the particle volume V. In the second relaxation process, the Néel relaxation, the magnetic moment changes its orientation within the particle overcoming the energy barrier constituted by the particles (crystal and shape) anisotropy resulting in an exponential relaxation time $\tau_N \sim \exp(V)$. Furthermore, real nanoparticle ensembles always contain a range of particle sizes, thereby leading to a superposition of exponential decays having different time constants.[3] MRX has been proven useful for localization, quantification, and imaging of magnetic nanoparticles inserted into biological tissue in medical applications such as magnetic drug targeting[14] or hyperthermia.[15] Iron oxide-based nanoparticles, usually suspended in an aqueous medium and encapsulated by an organic shell to enhance stability and biocompatibility, are most commonly used in such applications. We prepared a series of nanoparticle samples[16] with decreasing total iron content 400, 40, and 4 μg (140 μl total volume, stock suspension diluted 1:10, 1:100, and 1:1000 in distilled water and freeze-dried to suppress Brownian relaxation). Each sample was positioned 10 mm below the CSAM and magnetized for 3 s in a homogenous magnetic field of 1 mT. After the field had been turned off, the decaying residual magnetic field from the magnetic nanoparticles was recorded by the CSAM over 10 s with an inte-

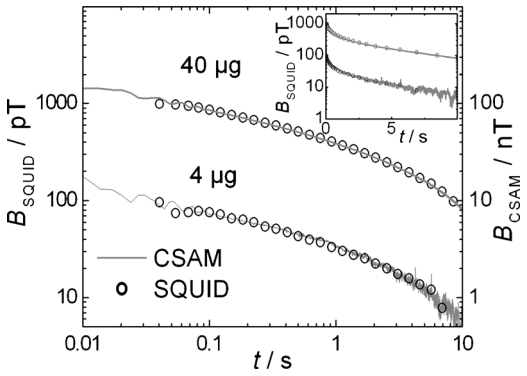

FIG. 3. Magnetic relaxation curves of two different nanoparticle concentrations (40 and 4 μg iron) derived from consecutive measurements by CSAM (solid line) and SQUID sensor (open dots). The inset shows the same data on a log-lin plot.

gration time constant of 300 μs, and the signal was digitized at 10 000 samples/s with an antialiasing filter below 5 kHz. Subsequently, the samples were magnetized under identical conditions and the field curves were measured with a SQUID sensor at a distance of 40 mm.

The relaxation curves of the 40 and 4 μg samples are displayed in a double-logarithmic plot in Fig. 3 for both sensor types. For graphical representation of B_{SQUID} and B_{CSAM}, the remanent magnetization $B(t=10\ \text{s})$ was subtracted and an offset of about 10% of the detected relaxation signal $[B(t=0.01\ \text{s})-B(t=10\ \text{s})]$ added for each decay curve. Then the CSAM data were scaled with a factor close to unity to shift the CSAM data onto the SQUID data for display purposes. Given unavoidable small errors in the sensor-sample distances a perfect scaling of the CSAM data onto the SQUID data or vice versa is not expected initially. From the SQUID sensor data only selected points of the logarithmically sampled relaxation curves are shown for better comparison with the CSAM data. Because of the proximity of the CSAM to the sample, the CSAM signal saturated for the high-mass 400 μg sample (curve not shown in Fig. 3). Within the measurement precision, the detected relaxation curves are identical. Independent of the total mass of iron in the magnetic nanoparticle sample, the shape of the relaxation curve is maintained. This behavior is expected for stable magnetic nanoparticles with negligible interaction and without aggregation. Furthermore, the superposition of a wide range of relaxation times becomes directly visible as a deviation of the curve shape from a straight line on a log-lin plot (see inset of Fig. 3). Even with this nonoptimized setup, MRX on a low-mass sample of 4 μg could be reliably observed with the CSAM. This demonstrates the capabilities of the CSAM and particularly its sensing stability over the measurement interval of tens of second.

While the performance of the CSAM used in these experiments was considerably better than that of other small portable room-temperature sensors, several improvements could still be made. When initially tested, this sensor performed at a level of roughly 100 to 200 $\text{fT}/\text{Hz}^{1/2}$ between 10 and 200 Hz. Considerably improved sensitivities have been achieved by use of more complicated optical configurations, which rely on optical polarimetry and large detuning to probe the orientation of the atoms.[4] Furthermore, as described above, magnetic fields produced by the CSAM sensors themselves can interfere with other sensors placed nearby. Fields produced by the electrical heaters can be eliminated by use of absorbed light from a laser to heat the cell.[17] The modulation field currently applied to the sensor head could be removed by implementing the method of polarization rotation, either by direct detection of the signal from a balanced polarimeter, which cancels most of the internal noise,[8] or through phase-sensitive detection through modulation of the probe light polarization.[11] Finally, because the microfabrication techniques used here are amenable to large-scale parallel fabrication of components, the current system is scalable to considerably larger numbers of sensor heads. It is estimated that roughly 100 sensors could be powered from a single pump and single heating laser. With respect to MCG such system enhancement would allow the operator to place multiple CSAMs freely at many positions near the chest, similar to the placement of ECG electrodes but without the problem of contact resistance. Packing the sensors in a dense array, with spacing of a few millimeters, would allow high-order gradiometry and the measurement of magnetic fields with high spatial resolution.

[1] K. Sternickel and A. I. Braginski, Supercond. Sci. Technol. **19**, S160 (2006).
[2] J. Clarke, M. Hatridge, and M. Mossle, Annu. Rev. Biomed. Eng. **9**, 389 (2007).
[3] D. Eberbeck, F. Wiekhorst, U. Steinhoff, and L. Trahms, J. Phys.: Condens. Matter **18**, S2829 (2006).
[4] H. B. Dang, A. C. Maloof, and M. V. Romalis, arXiv:0910.2206 (unpublished).
[5] H. Xia, A. Ben-Amar Baranga, D. Hoffman, and M. V. Romalis, Appl. Phys. Lett. **89**, 211104 (2006).
[6] G. Bison, N. Castagna, A. Hofer, P. Knowles, J. L. Schenker, M. Kasprzak, H. Saudan, and A. Weis, Appl. Phys. Lett. **95**, 173701 (2009).
[7] P. D. D. Schwindt, S. Knappe, V. Shah, L. Hollberg, J. Kitching, L.-A. Liew, and J. Moreland, Appl. Phys. Lett. **85**, 6409 (2004).
[8] W. C. Griffith, S. Knappe, and J. Kitching, Femtotesla atomic magnetometry in a microfabricated vapor cell. (unpublished).
[9] V. Shah, S. Knappe, P. D. D. Schwindt, and J. Kitching, Nat. Photonics **1**, 649 (2007).
[10] R. Mhaskar, S. Knappe, and J. Kitching, Proceedings of the IEEE International Frequency Control Symposium, Long Beach, CA, 2010, p. 376.
[11] J. C. Allred, R. N. Lyman, T. W. Kornack, and M. V. Romalis, Phys. Rev. Lett. **89**, 130801 (2002).
[12] A. Schnabel, M. Burghoff, S. Hartwig, F. Petsche, U. Steinhoff, D. Drung, and H. Koch, Neurol. Clin. Neurophysiol. **70**, 1 (2004).
[13] J. Bork, H.-D. Hahlbohm, R. Klein, and A. Schnabel, Proceedings of the 12th Internatonal Conference on Biomagnetism, Espoo, Finland, 2001, p. 970.
[14] P. Dames, B. Gleich, A. Flemmer, K. Hajek, N. Seidl, F. Wiekhorst, D. Eberbeck, I. Bittmann, Ch. Bergemann, Th. Weyh, L. Trahms, J. Rosenecker, and C. Rudolph, Nat. Nanotechnol. **2**, 495 (2007).
[15] H. Richter, M. Kettering, F. Wiekhorst, U. Steinhoff, I. Hilger, and L. Trahms, Phys. Med. Biol. **55**, 623 (2010).
[16] Resovist, Bayer Schering Pharma, c(Fe)=0.5 mol/l; liver-specific contrast agent for magnetic resonance imaging of focal liver lesions; reference for technical clarity and does not imply endorsement by NIST.
[17] J. Preusser, V. Gerginov, S. Knappe, and J. Kitching, Proceedings of the IEEE Sensors Conference, 2008, p. 344.